Apoptosis (2019) 24:745–755
https://doi.org/10.1007/s10495-019-01554-8

SPECT/CT imaging of apoptosis in aortic aneurysm with radiolabeled duramycin

Chengkai Hu[1,2] · Hui Tan[3,4,5] · Qingyu Lin[3,4,5] · Mieradilijiang Abudupataer[1,2] · Yun Zhao[1,2] · Jun Li[1,2] · Jiawei Gu[1,2] · Dengfeng Cheng[3,4,5] · Chunsheng Wang[1,2] · Kai Zhu[1,2] · Hao Lai[1,2]

Published online: 21 June 2019

Abstract

The objective of this research was to estimate whether a $^{[99mTc]}$duramycin probe can be used for apoptosis imaging in patients with aortic aneurysm (AA). Vascular smooth muscle cell (SMC) apoptosis has an important influence on AA development. Thus, non-invasive imaging of SMC apoptosis may be able to evaluate AA progress and risk stratification. SMCs were treated with hydrogen peroxide (H_2O_2; 200 μM) or culture medium as a control. Apoptosis was measured using flow cytometry and $^{[99mTc]}$duramycin to detect the binding efficiency to apoptotic SMCs. C57/BL6 mice were administered angiotensin-II and beta-aminopropionitrile (BAPN) subcutaneously to establish an AA model, or saline for controls. Aortic specimens underwent pathological evaluation and their aortic diameters were measured after 6 weeks. Micro-SPECT/CT scanning of $^{[99mTc]}$duramycin and ^{18}F-FDG PET detection were performed. SMCs treated with H_2O_2 showed more apoptosis compared with the control group ($67.2 \pm 3.8\%$ vs. $16.1 \pm 0.6\%$, $P < 0.01$). The experimental group showed a high rate of AA formation (70%) compared with no AA formation in the control group. The average aorta diameter was higher and $^{[99mTc]}$duramycin uptake at the AA site was higher in the experimental group compared with the control group. Compared with the normal aorta in the control group, AA in experiment group had more severe medial degeneration, elastic fiber reduction and fracture, and collagen degeneration. TUNEL staining verified the higher apoptosis rate at the AA site in experiment group compared with the control group ($63.9 \pm 3.7\%$ in ascending AA, $66.4 \pm 4.0\%$ in thoracic AA, vs. $3.5 \pm 0.3\%$ in normal aorta, $P < 0.01$). $^{[99mTc]}$Duramycin may be an effective probe to evaluate apoptosis in AA.

Keywords Duramycin · Aortic aneurysm · Apoptosis · Vascular smooth muscle cells · Micro-SPECT/CT

Introduction

Aortic aneurysm (AA) is a frequently occurring cardiovascular disease, and AA rupture is correlated with a high mortality rate. The characteristics of AA are aortic wall injury and progressive dilatation. Clinically, surgery is the main treatment strategy for AA [1, 2]. However, most AAs have no significant clinical symptoms and an uncertain progression, but when fatal complications or rupture occurs, the patient's prognosis is poor [3]. Currently, AA evaluation is mainly based on the aortic diameter size [4], which does not identify the early-stage or subclinical AA [5]. A detailed study of AA may identify predictors based on pathogenesis, which could be useful targets for monitoring AA progression [6–8]. Comprehensive pathological mechanisms are involved in AA, including inflammatory cell infiltration, SMC apoptosis, and extracellular matrix degradation, which could weaken the vessel's structural integrity and lead to

Chengkai Hu and Hui Tan have contributed equally to this work.

✉ Dengfeng Cheng
cheng.dengfeng@zs-hospital.sh.cn

✉ Kai Zhu
zhu.kai1@zs-hospital.sh.cn

✉ Hao Lai
lai.hao@zs-hospital.sh.cn

1 Department of Cardiac Surgery, Zhongshan Hospital, Fudan University, 1609 Xietu Road, Shanghai 200032, China

2 Shanghai Institute of Cardiovascular Diseases, Shanghai 200032, China

3 Department of Nuclear Medicine, Zhongshan Hospital, Fudan University, 180 Fenglin Road, Shanghai 200032, China

4 Institute of Nuclear Medicine, Fudan University, Shanghai 200032, China

5 Shanghai Institute of Medical Imaging, Shanghai 200032, China

aneurysm progression [9]. SMCs, which are the predominant effector cells in the aorta tunica media, have a vital function in maintaining vascular wall structure and function [10, 11]. SMC apoptosis contributes to the weakening of vessel structural integrity and has been considered to be an effective predictor of AA progression [12]. Therefore, imaging SMC apoptosis could be helpful to evaluate the extent of structural injury during AA progression and provide guidance for risk stratification.

Duramycin is a new type of apoptosis probe, which is a small molecular weight protein that binds specifically to phosphatidylethanolamine (PE) [13, 14]. [^{99m}Tc]-Duramycin accumulates strongly in target tissues in a PE-dependent fashion [15]. Radiolabeled duramycin has been used extensively in apoptosis imaging in tumors, atherosclerosis, and ischemia–reperfusion injury [14, 16, 17]. In this research, we evaluated whether [^{99m}Tc]duramycin can be an imaging probe to evaluate apoptosis in AA development.

Methods

Duramycin radiolabeling

As previously reported, 150 µL of sodium acetate buffer (pH 5.3) was added in a single-step kit composed of 15 µg hydrazinonicotinamide (HYNIC)-duramycin for Tc-99 m labeling. In a 1.5-mL centrifuge tube, 30 µL (3 µg) HYNIC-duramycin solution and 100 µL freshly prepared [^{99m}Tc]-pertechnetate (222 MBq) in 100 µL of saline was added at 80 °C for 20 min. This probe's radiochemical purity was tested using Radio-TLC using two separate chromatography systems. System 1 comprised 20% NaCl that was placed onto silica gel-impregnated paper that was cut into 1 cm × 10 cm strips, and system 2 was distilled water. In system 1, free [^{99m}Tc]-pertechnetate and impurities migrated up the solvent front, whereas reduced Tc-99 m and [^{99m}Tc]duramycin remained at the origin. In system 2, free [^{99m}Tc]-pertechnetate, impurities, and [^{99m}Tc]duramycin migrated to the solvent front, but the hydrolyzed reduced Tc-99m stayed at the origin.

Cell culture

CRL-1999 T/G HA-VSMC, which were purchased from American Type Culture Collection (Manassas, VA, USA) were grown in DMEM/F12 at 37 °C with 5% CO_2. Then, 10% FBS and 1% antibiotics were added into the medium. Cell viability was tested using light microscopy.

In vitro apoptosis in SMCs assessed using flow cytometry

For apoptosis analysis, SMC suspension was inoculated into wells on six cell culture plates, at a concentration of approximately 3×10^5 cells/well. Three culture wells, which were treated with a concentration of 200 µM hydrogen peroxide (H_2O_2) in DMEM/F12 at 37 °C in a moist atmosphere were the experimental groups, and the other three culture wells without H_2O_2 treatment were used as the control groups. After a 30-min incubation, cells were separated from the medium, washed with phosphate buffer saline (PBS), and centrifuged for 5 min at 1000 rpm. After the cells were resuspended in binding buffer, a cell suspension that was treated with 3 µL APC-Annexin V and 3 µL PI, was incubated at 20 °C in dark conditions for 30 min. The cells were then checked using flow cytometry. This protocol is summarized in Fig. 1a.

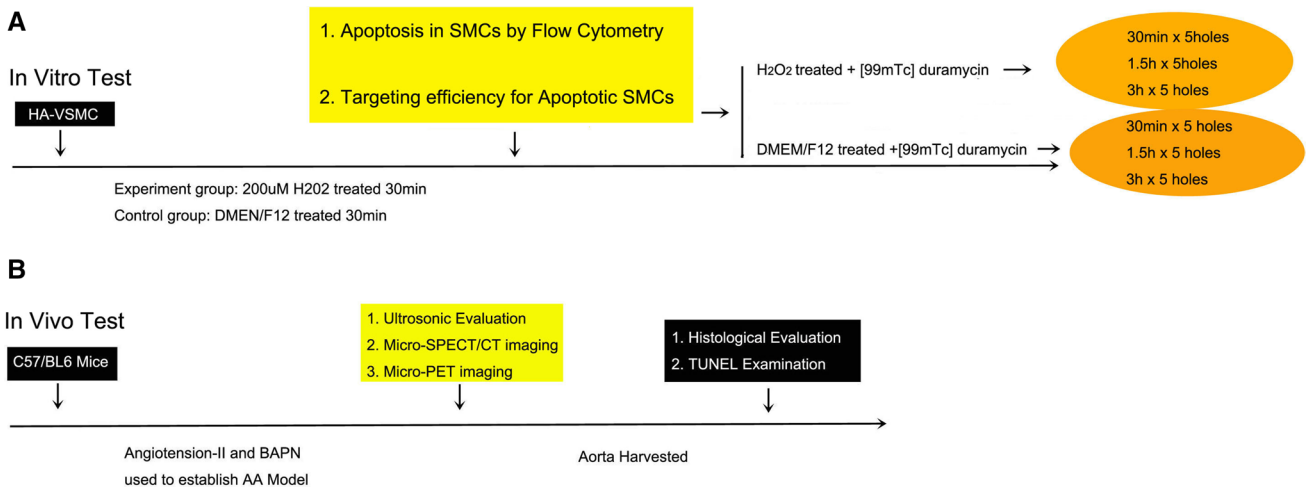

Fig. 1 Experimental Protocol. **a** In vitro tests for evaluating SMC apoptosis and duramycin binding. **b** In vivo tests for evaluating [^{99m}Tc]duramycin imaging in a mouse AA model

In vitro targeting efficiency for apoptotic SMCs

To evaluate $^{[99mTc]}$duramycin efficiency for apoptotic SMCs, we divided SMCs into experimental and control groups. The SMCs (average of 3×10^5 cells/well) were counted and plated onto 24-well culture plates. Following cell adherence, the SMCs in the experimental group were treated with 200 μM H_2O_2 to stimulate apoptosis. The control group contained SMCs that were treated with DMEM/F12. After a 30-min incubation, the H_2O_2 and DMEN/F12 were discarded and 0.01 M phosphate buffered saline (PBS) was used to rinse the cells. $^{[99mTc]}$Duramycin with a specific activity of 1 μg/74 MBq was added to the experimental and control wells, and 500 μL serum-free medium was then added to each well. After incubation for 30 min, 1.5 h, or 3 h, we measured the cell-binding rate of apoptotic SMCs at each time point based on the method described below: (1) Supernatant was removed and added to test tube No. 1 and 500 μL of 0.01 M cold PBS was used to wash each well (twice for 2 min each). The supernatant was then added to test tube No. 1, which was called the cell junction tube; 2) Trypsin–EDTA (1×; 500 μL; 0.25%) was added into each well and incubated for 15 min. When the adherent cells were completely lysed, the lysate was transferred to test tube No. 2, and each well was then washed with 500 μL of 0.01 M cold PBS (twice for 2 min each). The supernatant was also added to test tube No. 2, which was called the cell-unbounded tube; and 3) The CPM values of each tube, the cell binding rate (%), and cell binding (mol/cell) were measured using a γ-counter (CRC-15R, Capintec Inc., Ramsey, NJ, USA). The equation is as follows: cell binding rate (%) = CPM of cell junction/(CPM of cell junction + CPM of cell-unbounded) × 100%. Each group comprised five replicates and the protocol is summarized in Fig. 1a.

Animal model

C57/BL6 mice (male, 8 weeks old) were purchased from Shanghai SLAC Laboratory Animal Co. Ltd. (Shanghai, China). An osmotic pump (Alzet, Cupertino, CA, USA) was implanted in 20 mice to form aneurysms in vivo [18]. The osmotic pump containing angiotensin-II (1000 ng/kg/min; ApexBio, Boston, MA, USA) was placed subcutaneously to release drugs for 6 weeks and BAPN (150 mg/kg/day; Energy Chemical, Shanghai, China) was placed subcutaneously to release drugs for 2 weeks in the experimental group. The control group comprised four mice that were treated in the same manner except that physiological saline was administered. BAPN is a lysine oxidase inhibitor that has an important function in degrading the elastic membrane in the AA model [19]. The protocol is summarized in Fig. 1b.

Ultrosonic evaluation

The aortic diameter was assessed in mice that survived after 6 weeks of treatment. Assessments were made using a small animal ultrasonic instrument under 2% isoflurane respiration anesthesia. The aortic diameter change was observed in the ascending aorta and abdominal aorta.

Micro-SPECT/CT imaging and data analysis

All surviving mice were treated with $^{[99mTc]}$duramycin (18.5 MBq/0.5 μg per mouse) via a caudal vein injection. 2 h after this injection, mice were placed into a micro-single photon emission computed tomography/computed tomography (Micro-SPECT/CT) scanner (Bioscan, Washington DC, USA) for SPECT/CT imaging under 2% isoflurane respiration anesthesia. The main CT parameters were as follows: tube voltage, 45 keV; tube current, 0.15 mA; exposure time, 500 ms/frame; and frame resolution, 256 × 512. The main SPECT parameters were as follows: scanning time, 35 s/projection; energy peak, 140 keV; window width, 10%; matrix, 256 × 256; and resolution, 1 mm/pixel. The SPECT and CT images for mice were acquired at the same location. Data were reconstructed using the HiSPECT algorithm. The next day, mice were fasted for 6 h were then subjected to micro-PET imaging. ^{18}F-FDG (7.4–11.1 MBq per mouse) was injected through the tail vein. 1 h later, mice were placed on a micro-PET scanner (Metis PET; Shandong Maide Yinghua Technology Co., Ltd., Shandong, China). The main parameters concluded: FOV (Transaxial), 80 mm; FOV(Axial), 59 mm; spatial resolution, < 1.3 mm; and peak, 226 Kcp. The protocol is summarized in Fig. 1b.

The post-processing of data was completed by using software InVivo Scope (Version 1.43, Bioscan, Washington DC, USA). 3D region of interest (ROI) was drawn in the site of AA formation, the site of aorta without AA formation in the AA formation mouse and the site of aorta in the control mouse, while the background ROIs with similar diameter were drawn in the site of surrounding muscle. We selected three ROIs for each site and concentration of radioactivity of each ROI (μCi/mm^3) was calculated by the software. The lesion-to-background ratio (L/B) was used to express lesion signal intensity, aiming to reduce inter-mice variations.

Ex vivo planar imaging

After 6 weeks intervention, we selected three experiment mice and three control mice to test the excised aortas for ex vivo planar imaging by breast specific gamma imaging (BSGI) with a high resolution, to eliminate adjacent tissue interference and further confirm signal intensity. All six mice were treated with $^{[99mTc]}$-duramycin (18.5 MBq/0.5 μg per mouse) via a caudal vein injection. 2 h after this injection,

all mice were anesthetized using an intraperitoneal injection of 3% pentobarbital and the complete aorta were harvested and washed by saline, then the aorta was placed into BSGI scanner, the main parameters were as following: collimator, low-energy general-purpose; peak energy, 140 keV; window width, 10%; resolution, 0.32 mm/pixel; matrix, 80 × 80. The collection time was 20 min. The semi-quantitative analysis of $^{[99mTc]}$-duramycin uptake in BSGI of aortic aneurysm was view as the lesion to background counts ratio (L/B).

Histological evaluation

After PET/CT imaging, all surviving mice were anesthetized using an intraperitoneal injection of 3% pentobarbital. After exposing the heart, the right atrial appendage was cut and 0.9% saline and 4% neutral formaldehyde were perfused at the apex of heart. The complete aorta was exposed and an overall general image was obtained using a digital camera, and the aorta was then harvested and fixed in 4% neutral formaldehyde. The aorta specimens were sectioned at a thickness of 5 mm after being embedded in paraffin. Van Gieson (VG), Elastica van Gieson (EVG), and hematoxylin and eosin (H&E) staining were used for histochemical examination. The protocol is summarized in Fig. 1b.

The pathological aortic sections were used for TdT-mediated dUTP Nick-End Labeling (TUNEL) examination. A TdT and dUTP in a TUNEL kit (Roche) were mixed at a ratio of 1:9 to cover the tissue and incubated in a 37 °C incubator for 2 h. The slices were then washed with PBS (pH 7.4) three times for 5 min each. After removing PBS, DAPI dye solution was added to the tissue and incubated in the dark for 10 min. Images were observed and collected under a fluorescence microscope (DAPI ultraviolet excitation wavelength, 330–380 nm; emission wavelength, 420 nm, blue light; FITC excitation wavelength, 465–495 nm, emission wavelength, 515–555 nm, green light; CY3 excitation wavelength, 510–560, emission wavelength, 590 nm, red light). The protocol is summarized in Fig. 1b.

Statistics

GraphPad Prism 6.01 and SPSS version 22 were used for statistical analysis. The imaging processing was performed using Adobe Photoshop 6.2. The numerical value was presented as the mean ± standard deviation (SD). $P < 0.05$ was considered to be as statistically significant.

Results

In vitro cell test

We found that SMCs in the control group were mainly normal compared with those in the H_2O_2-treated group; SMCs in the experimental group were mainly in the apoptotic state (Fig. 2a, b). The SMC apoptosis rate in H_2O_2-treated cells was significantly higher than SMCs that were not treated with H_2O_2 (67.2 ± 3.8% vs. 16.1 ± 0.6%, $P < 0.01$; Fig. 2c).

In vitro targeting efficiency for apoptotic SMCs

The H_2O_2-treated SMCs has a higher uptake of $^{[99mTc]}$duramycin compared with the control group at 0.5, 1, and 3 h (Fig. 3). The average uptake percentage of $^{[99mTc]}$duramycin was 1.4 ± 0.5% and 0.2 ± 0.1% in the H_2O_2-treated and control groups, respectively ($P < 0.01$).

Animal models of aortic aneurysm

There were 14 (14/20) AAs in mice in the experimental group, which included seven mice that died from ruptured AAs or aortic dissection (7/14) (Fig. 4a). Among ruptured and unruptured AAs, 20% (4/20) of mice developed an

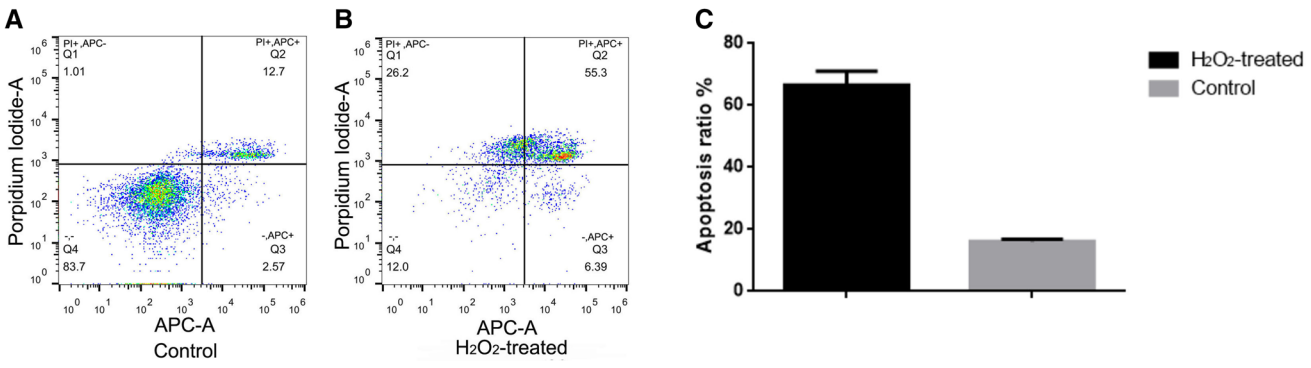

Fig. 2 In vitro tests for evaluating apoptosis in SMCs. **a** The control group that was not treated with H_2O_2 did not show significant apoptosis and most SMCs were normal. **b** SMCs in H_2O_2-treated group were mainly in the apoptotic state. **c** The apoptosis rate in the H_2O_2-treated group was significantly higher compared with the control group (67.2 ± 3.8% vs. 16.1 ± 0.6%, $P < 0.01$)

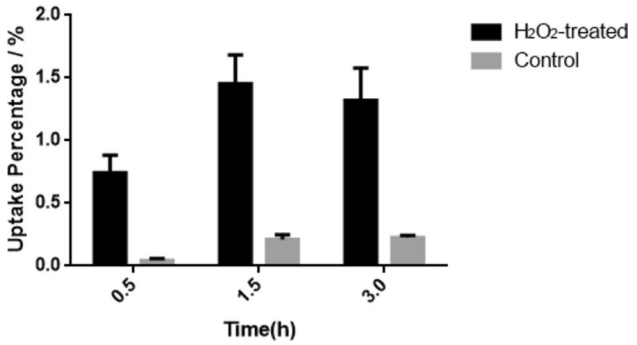

Fig. 3 Measurements of in vitro targeting ability of [99mTc]duramycin. The H_2O_2-treated SMCs group had a higher apoptotic SMC uptake percentage of [99mTc]duramycin compared with the control group (1.4 ± 0.5% vs. 0.2 ± 0.1%, $P < 0.01$)

ascending AA, 25% (5/20) of mice developed a thoracic AA (TAA), and 25% (5/20) developed an abdominal AA (AAA; Fig. 4b). After 6 weeks, the aortic diameter was assessed in all the surviving mice using a small animal ultrasonic instrument using 2% isoflurane respiration anesthesia. The ascending aortic and abdominal aorta layers were assessed. The aorta in the experimental group was significantly dilated (Fig. 4c). The aortic mean diameter in the experimental group was 1.8 ± 0.2 mm, and in control group, it was 1.0 ± 0.1 mm, which was significantly different ($P < 0.01$; Fig. 4d). The expansion ratio was up to 50%. On ^{18}F-FDG imaging, we found that AAs in the experimental group (Fig. 4e a, b) had more positive imaging compared with the control group (Fig. 4e c, d).

Imaging of apoptosis in an aortic aneurysm

Based on the imaging tests, we found that the radioactivity of [99mTc]duramycin was increased at the site of AA formation in the experimental group (Fig. 5b, c), and the control group had no positive imaging (Fig. 5a). Additionally, the uptake of [99mTc]duramycin at the AA site in the AA group was higher compared with the control group (4.53 ± 1.89 vs. 1.41 ± 0.37, $P = 0.001$, Fig. 5d) and non-AA site in AA group (4.53 ± 1.89 vs. 1.38 ± 0.41, $P = 0.002$, Fig. 5d). Moreover, there was no significant difference between non-AA site in AA group and control group on the uptake of [99mTc]duramycin (1.38 ± 0.41 vs. 1.41 ± 0.37, $P = 0.85$, Fig. 5d).

Ex vivo planar imaging

From the ex vivo planar imaging, we found the AA site in the experiment group had obviously positive imaging and the control mice with negative imaging at the same site (Fig. 6a, b). The semi-quantitative analysis of [99mTc]duramycin showed that the L/B ratio in experiment group was significantly higher than control group (11.3 ± 1.25 vs. 6.4 ± 0.89, $P < 0.01$, Fig. 6c).

Histological evaluation

Histological evaluation results of control and experimental aortae are shown in Fig. 7. We chose two layers of the control and experiment aortae. Compared with the control aorta, we found that aorta with AAs showed severe medial degeneration, elastic fiber reduction and fracture, and collagen degeneration (Fig. 7).

Tunel evaluation

The outcomes of the apoptosis test are shown in Fig. 8. Figure 8a shows the TUNEL examination imaging in the control group, ascending AA, and TAA. The left picture is DAPI dye, which has a blue color, the middle picture has multiple dyes, the right picture is the FITC-TUNEL dye, which has a green color. Through TUNEL examination, we found positive apoptosis imaging in the aorta, which had AA formation (Fig. 8a). However, the control aorta has negative apoptosis imaging. Compared with aortae in the control group, the ascending AA and TAA had a significantly higher ratio of apoptotic cells (3.5 ± 0.3% vs. 63.9 ± 3.7%, 66.4 ± 4.0%, $P < 0.01$, Fig. 8b).

Discussion

AA is a fatal cardiovascular disease with an acute onset and rapid development. AAs are often found with dissection or an obvious pulsatile lump resulting from their usually hidden onset and no obvious clinical symptoms. Currently, AA diagnosis is usually based on CT imaging to estimate the dilated aortic diameter, but AAs in their early stages cannot be clearly identified in a clinical scenario.

AA animal models have been constructed using many strategies, including chemical induction and genetic mutation. In the present study, we selected BAPN and angiotensin-II to induce AA. Lysine oxidase has vital function in maintaining the strength of the elastic lamina [20]. BAPN, a lysine oxidase inhibitor, can cause degeneration of elastic laminas that reduce the strength of the aortic wall. Combined with angiotensin-II, BAPN can induce aortic wall dilation. In this study, we found that this model has a good AA formation rate and an acceptable mouse mortality rate. Previous experimental models selected include ApoE$^{-/-}$ mice or LDL$^{-/-}$mice with high fat diet that were used in atherosclerosis studies [21, 22], but the ratio of AA formation was low and the AA usually occurred after mature atherosclerotic lesions are formed, which takes a long time. Additionally, elastase infusion, calcium chloride, and angiotensin-II

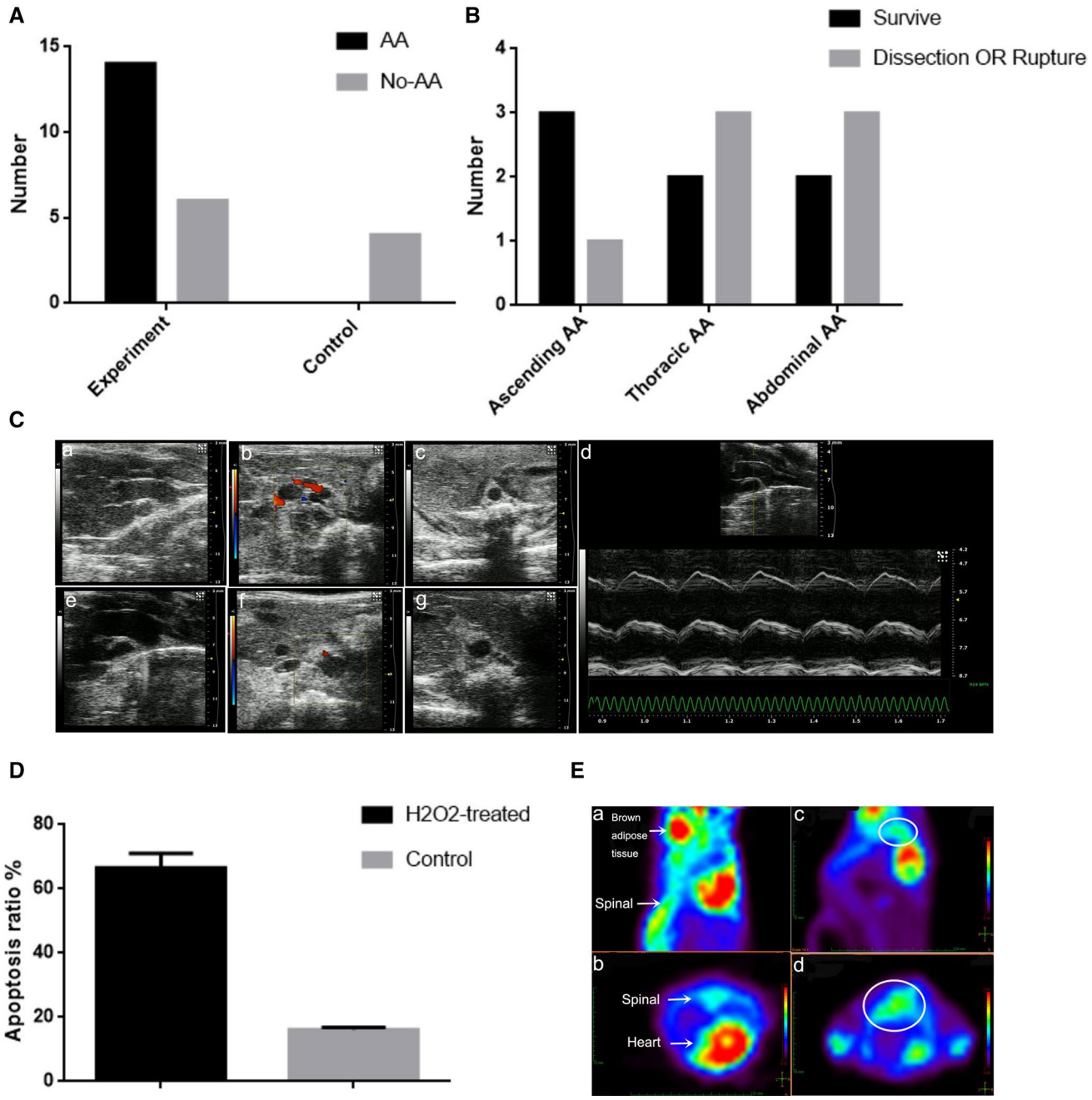

Fig. 4 Aortic aneurysm formation in mice using BAPN and angiotensin-II. **a** The incidence of AA formation was significantly different between the experimental and control groups. The overall AA incidence was 70% (14/20). **b** The types of AA in the experimental group were ascending AA (4/14), TAA (5/14), and AAA (5/14). The survival rate of patients with AAs was 75, 40, and 40% in the three groups, respectively. **C** Diameters of the ascending and abdominal aorta were larger in the experimental group (e–g) compared with the control group (a–c). M-mode echocardiography in AAs is shown in d. **d** The aortic diameter was visibly larger in the experimental group compared with the control group (1.8 ± 0.2 mm vs. 1.0 ± 0.1 mm, $P < 0.01$). **e** ^{18}F-FDG uptake in AA (a and b) AA is higher than in the control group (c and d). The white circle indicates positive imaging

are the common ways to induce AA formation [23–25]. Although local application of calcium chloride can induce AA quickly, it requires opening the chest and exposing the aorta, which may cause surgical death and it is not a suitable model to use with a large number of subjects. In the animal model used in this study, angiotensin-II and BAPN simulate the physiological mechanism of hypertension that produces aneurysms and they can induce aneurysms at multiple sites rather than at a single site. Therefore, Ang-II and BAPN-induced AA in mice is a suitable animal model to enable

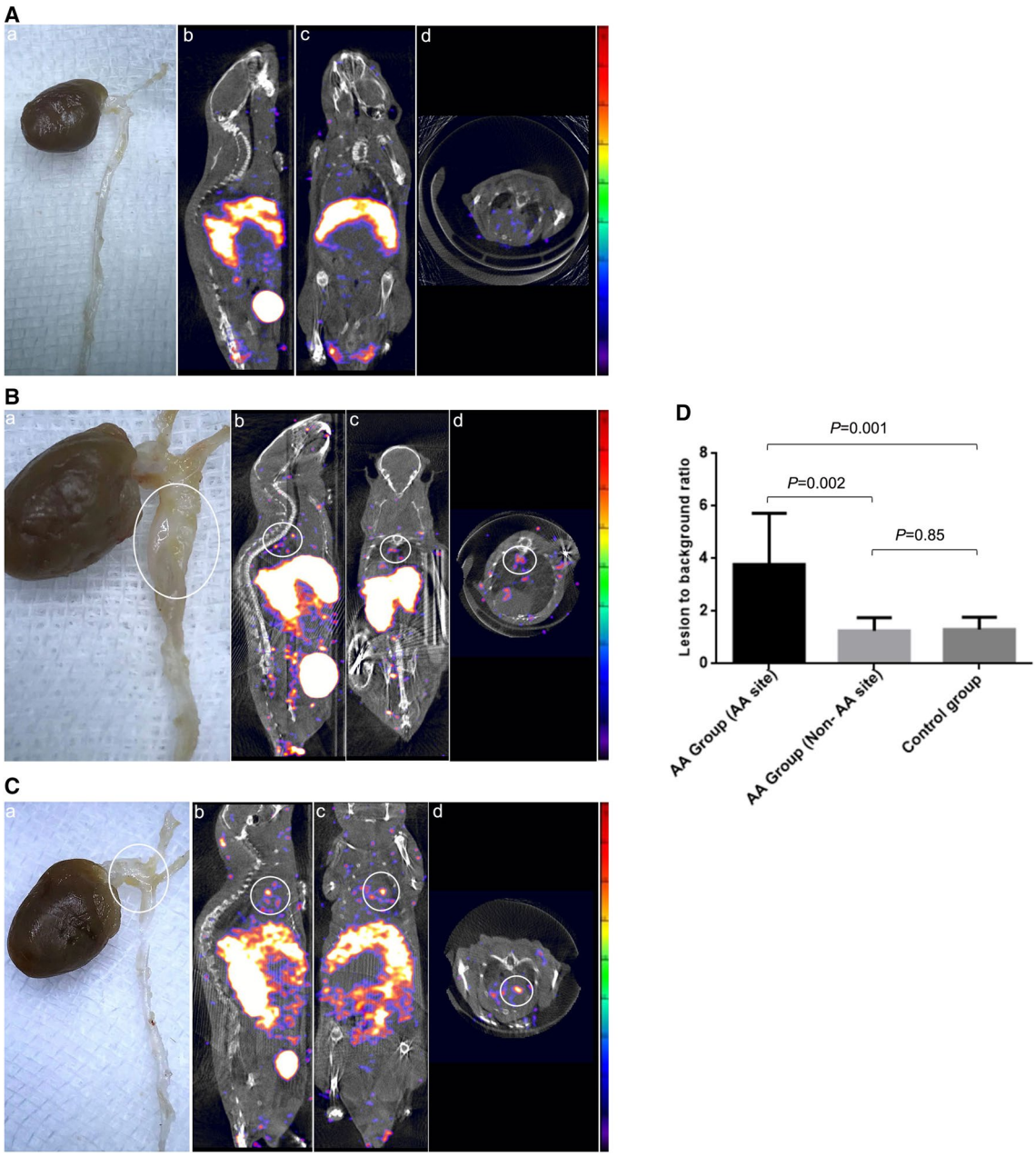

Fig. 5 Image of AA in SPECT/CT. The [99mTc]duramycin of micro-SPECT/CT images in the control group (**a**) TAA (**b**) and ascending AA (**c**), quantitative analysis of L/B on SPECT/CT (**d**): the dilation of the aortic lumen in B and C. (b–d) [99mTc]duramycin uptake at 2 h post-intravenous injection at B and C. The control group had no visible positive imaging in A. **d** The uptake of [99mTc]duramycin at the AA site was higher compared with the control group ($P=0.001$) and non-AA site in AA group ($P=0.002$). Moreover, there was no significant difference of the uptake of [99mTc]duramycin between non-AA site in AA group and control group ($P=0.85$)

exploration of potential molecular imaging strategies at different AA sites.

Duramycin is a small protein that is composed of 19 amino acids and has a molecular weight of 2 kDa. Combined with a high PE sensitivity, it has proper tissue permeability, faster tissue clearance rate, and higher apoptosis targeting sensitivity. PE and phosphatidylserine (PS) mainly exist in the intracellular cell membrane. When cell death occurs [13, 15], it redistributes to the outer cell membrane and becomes the molecular targets for apoptosis [26, 27]. Thus, radiolabeled duramycin has been used in myocardial ischemia, atherosclerosis, and tumor imaging [14, 17]. Compared with annexin V, a 36-kDa human protein with 319 amino acids that binds to PS with a specific affinity, duramycin has a lower molecular weight, higher affinity for PE and fast clearance. In this study, we found that the

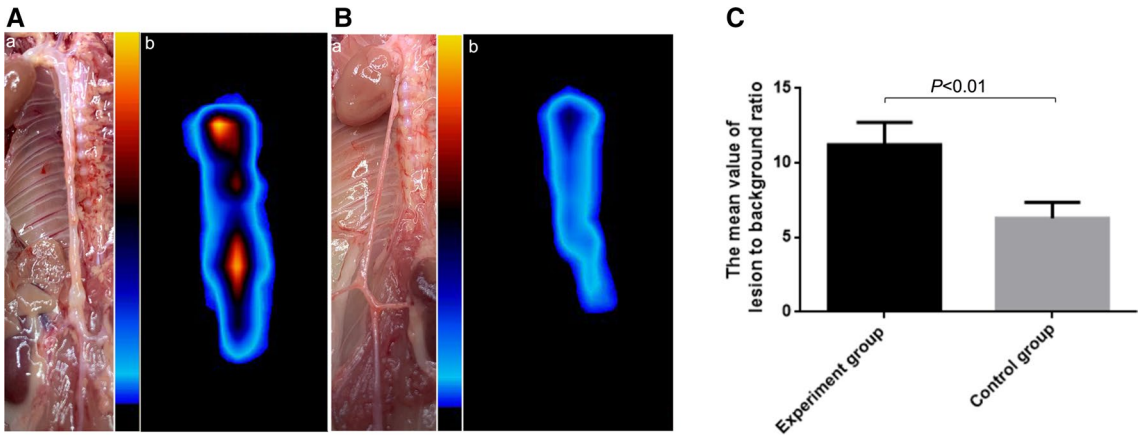

Fig. 6 The planar imaging of aorta. **a**, **b** BSGI imaging showed that the AA site in experiment group had positive imaging compared with control group. **c** The L/B in experiment group was significantly higher than control group (11.3 ± 1.25 vs. 6.4 ± 0.89, P < 0.01)

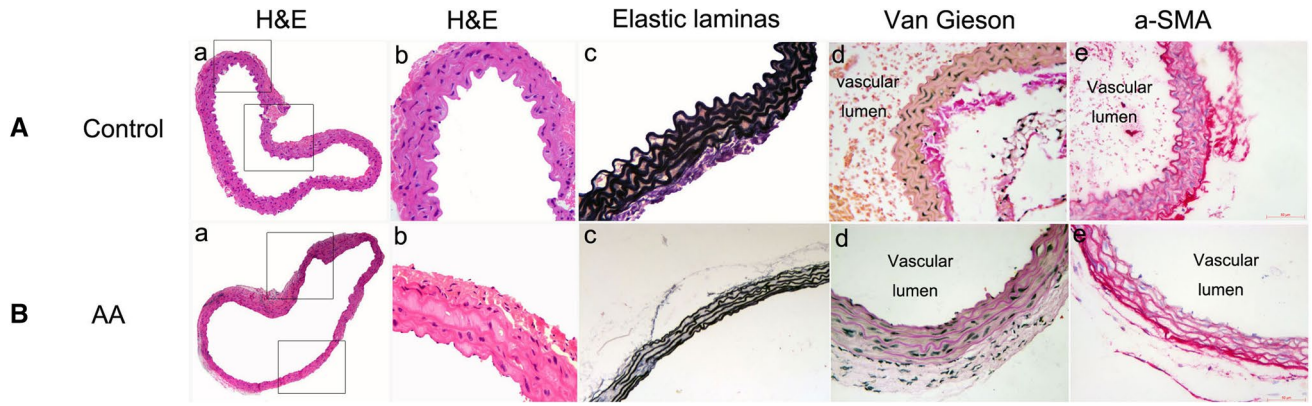

Fig. 7 The lumen of AA and control aortae showing the histological characteristics. [control (**a**); AA (**b**); a–e in order]: control aorta and AA were stained with H&E, elastic laminas, van Gieson, and α-SMA. Compared with control aorta, the AA had visible medial degeneration, elastic fiber fracture, and extracellular matrix degradation. Scale bar: 0.1 mm

uptake percentage of $^{[99mTc]}$duramycin in apoptotic SMCs was higher in the H_2O_2-treated group compared with the untreated group (1.4 ± 0.5% vs. 0.2 ± 0.1%, $P < 0.01$). Moreover, SMC apoptosis, which was vital for maintenance of the aortic structure, has an important influence in AA formation and progression. Studies have shown that AA development was accompanied by increased apoptosis in SMCs and AA progress with the development of more apoptosis [12, 28, 29]. One study has confirmed that up-regulated H19 induced SMC apoptosis and AA growth; moreover, the AA growth and SMC apoptosis were attenuated by inhibiting the H19 expression [12]. Additionally, another study found that there was more SMC apoptosis in a $CaPO_4$ AA model, which had greater AA dilation compared with the $CaCl_2$ model, which had a smaller diameter [28]. Our study also confirmed that AAs showed more apoptosis than a control model using the TUNEL test. Thus, SMC apoptosis may be a new tool to assess AA appearance and development.

With research progressing on the mechanism of aneurysm formation and pathology, many new methods to detect AA are emerging. Studies have shown that ^{18}F-FDG can be used to assess AA formation through absorption of ^{18}F-FDG into inflammatory tissues, which results from the inflammatory response during AA formation [30–32]. Ultra-small super-paramagnetic iron oxide (USPIO) imaging in MRI and variations in inflammatory mediators and the extracellular matrix can also assess the progress of AA [10, 33, 34]. Here, we selected ^{18}F-FDG imaging to verify whether our AA model was successfully established and we found more ^{18}F-FDG uptake at the AA site compared with the normal aorta (Fig. 4e). Additionally, based on the mechanism of SMC apoptosis in the formation of AAs and the higher sensitivity of duramycin toward apoptosis, we selected SPECT/CT to image apoptosis using $^{[99mTc]}$duramycin. Using this method, we found positive apoptosis signals in the area of AA formation and negative

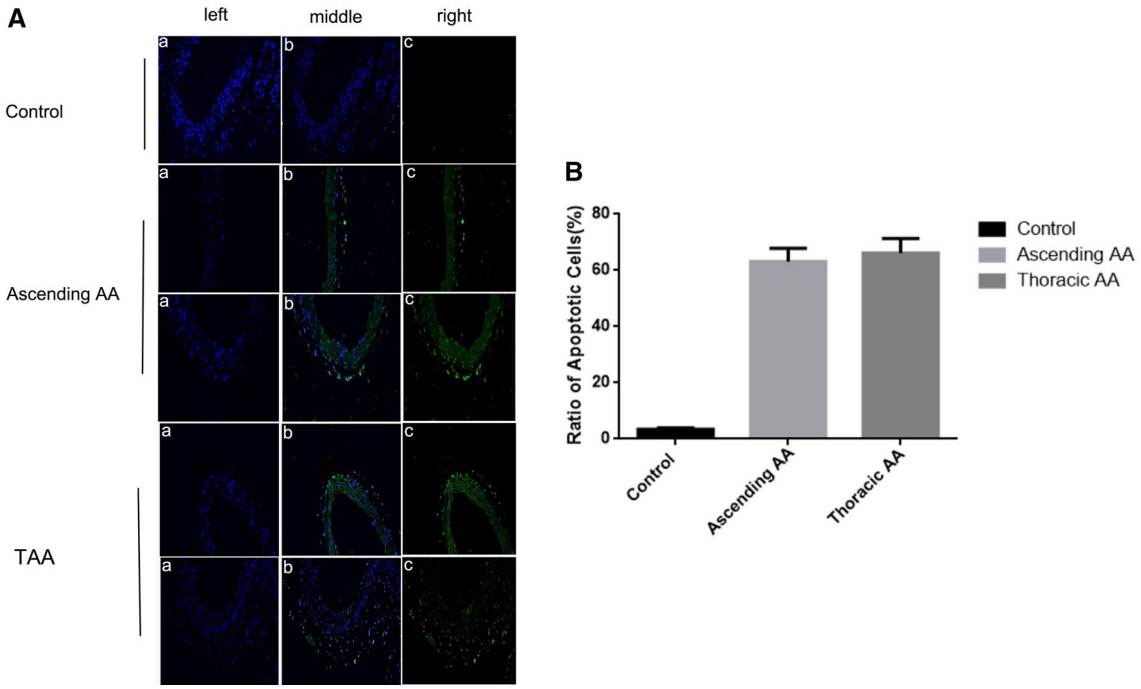

Fig. 8 Fluorescence TUNEL staining of aortic tissue acquired from control and experiment C57BL/6 mice. **a** From left to right, the panels show DAPI nuclear staining (blue), multiple staining, and FITC–TUNEL for apoptosis nuclear staining (green), respectively. There is a higher amount of positive staining in both the ascending aortic aneurysm and TAA compared with the control group. **b** Compared with aortae in the control group, the ascending AA and TAA had a significantly higher ratio of apoptotic cells ($3.5 \pm 0.3\%$ vs. $63.9 \pm 3.7\%$, $66.4 \pm 4.0\%$, $P < 0.01$)

signals in the control group (Fig. 5). In addition, we used BSGI to test the ex vivo imaging to verity the specificity of $^{[99mTc]}$duramycin and found AA site had positive imaging, but the control aorta without positive imaging at the same site (Fig. 6a, b). Moreover, the L/B in experiment group was significantly higher than control group (11.3 ± 1.25 vs. 6.4 ± 0.89, $P < 0.01$, Fig. 6c). In the pathological section, we selected the layer of AA and normal aorta to confirm the apoptosis level, and we found that ascending AA and TAA had a higher ratio of apoptotic cells compared with the normal aorta ($63.9 \pm 3.7\%$ and $66.4 \pm 4.0\%$ vs. $3.5 \pm 0.3\%$, $P < 0.01$, Fig. 8).

The outcomes of our study further verified the importance of SMC apoptosis in AA appearance and development. Because SMC apoptosis plays a central role in AA appearance and development of larger AAs, we suggest that early diagnosis of AA and evaluation of the risk factors for AA dilation may be assessed more comprehensively using $^{[99mTc]}$duramycin detection. This method may have the ability to show the pre-clinical stage of AAs, which have no obvious symptoms and negative imaging findings. This method may help clinicians to screen patients for high-risk factors for AA dilation or dissection and implement early intervention. However, further research is required to confirm our findings.

Conclusions

$^{[99mTc]}$Duramycin is a sensitive apoptosis probe, and it may be a new method for imaging of apoptosis in AA and for predicting the pathological progress. However, further studies are required to verify its application in early stages of AA.

Acknowledgements The authors acknowledge the funding from National Natural Science Foundation of China (Grant No. 81771971), Shanghai Pujiang Program (Grant No. 17PJ1401500), Shanghai Municipal Health Commission (Grant No. 201640134), and the "Chen Guang" Project Supported by Shanghai Municipal Education Commission and Shanghai Education Development Foundation (Grant No. 14CG06).

References

1. Clouse WD, Hallett JW Jr, Schaff HV, Gayari MM, Ilstrup DM, Melton LJ 3rd (1998) Improved prognosis of thoracic aortic aneurysms: a population-based study. JAMA 280(22):1926–1929. https://doi.org/10.1001/jama.280.22.1926
2. Ramanath VS, Oh JK, Sundt TM 3rd, Eagle KA (2009) Acute aortic syndromes and thoracic aortic aneurysm. Mayo Clin Proc 84(5):465–481. https://doi.org/10.1016/S0025-6196(11)60566-1
3. Clouse WD, Hallett JW Jr, Schaff HV, Spittell PC, Rowland CM, Ilstrup DM, Melton LJ 3rd (2004) Acute aortic dissection:

population-based incidence compared with degenerative aortic aneurysm rupture. Mayo Clin Proc 79(2):176–180. https://doi.org/10.4065/79.2.176
4. Johnston KW, Rutherford RB, Tilson MD, Shah DM, Hollier L, Stanley JC (1991) Suggested standards for reporting on arterial aneurysms. Subcommittee on reporting standards for arterial aneurysms, Ad Hoc Committee on reporting standards, society for vascular surgery and North American chapter, International society for cardiovascular surgery. J Vasc Surg 13(3):452–458. https://doi.org/10.1067/mva.1991.26737
5. Brown LC, Powell JT, UK Small Aneurysm Trial Participants (1999) Risk factors for aneurysm rupture in patients kept under ultrasound surveillance. Ann Surg 230(3):289–296 **(discussion 296–287)**
6. Akai A, Watanabe Y, Hoshina K, Obitsu Y, Deguchi J, Sato O, Shigematsu K, Miyata T (2015) Family history of aortic aneurysm is an independent risk factor for more rapid growth of small abdominal aortic aneurysms in Japan. J Vasc Surg 61(2):287–290. https://doi.org/10.1016/j.jvs.2014.07.007
7. Baxter BT, Davis VA, Minion DJ, Wang YP, Lynch TG, McManus BM (1994) Abdominal aortic aneurysms are associated with altered matrix proteins of the nonaneurysmal aortic segments. J Vasc Surg 19(5):797–802 **(discussion 803)**
8. Brophy CM, Reilly JM, Smith GJ, Tilson MD (1991) The role of inflammation in nonspecific abdominal aortic aneurysm disease. Ann Vasc Surg 5(3):229–233. https://doi.org/10.1007/BF02329378
9. Kuivaniemi H, Ryer EJ, Elmore JR, Tromp G (2015) Understanding the pathogenesis of abdominal aortic aneurysms. Expert Rev Cardiovasc Ther 13(9):975–987. https://doi.org/10.1586/14779072.2015.1074861
10. Shimizu K, Mitchell RN, Libby P (2006) Inflammation and cellular immune responses in abdominal aortic aneurysms. Arterioscler Thromb Vasc Biol 26(5):987–994. https://doi.org/10.1161/01.ATV.0000214999.12921.4f
11. Hu C, Zhu K, Li J, Wang C, Lai L (2017) Molecular targets in aortic aneurysm for establishing novel management paradigms. J Thorac Dis 9(11):4708–4722. https://doi.org/10.21037/jtd.2017.10.63
12. Li DY, Busch A, Jin H, Chernogubova E, Pelisek J, Karlsson J, Sennblad B, Liu S, Lao S, Hofmann P, Backlund A, Eken SM, Roy J, Eriksson P, Dacken B, Ramanujam D, Dueck A, Engelhardt S, Boon RA, Eckstein HH, Spin JM, Tsao PS, Maegdefessel L (2018) H19 induces abdominal aortic aneurysm development and progression. Circulation 138(15):1551–1568. https://doi.org/10.1161/CIRCULATIONAHA.117.032184
13. Zhao M, Li Z, Bugenhagen S (2008) 99 mTc-labeled duramycin as a novel phosphatidylethanolamine-binding molecular probe. J Nucl Med 49(8):1345–1352. https://doi.org/10.2967/jnumed.107.048603
14. Elvas F, Vangestel C, Rapic S, Verhaeghe J, Gray B, Pak K, Stroobants S, Staelens S, Wyffels L (2015) Characterization of [(99m)Tc]duramycin as a SPECT imaging agent for early assessment of tumor apoptosis. Mol Imaging Biol 17(6):838–847. https://doi.org/10.1007/s11307-015-0852-6
15. Audi S, Li Z, Capacete J, Liu Y, Fang W, Shu LG, Zhao M (2012) Understanding the in vivo uptake kinetics of a phosphatidylethanolamine-binding agent (99m)Tc-Duramycin. Nucl Med Biol 39(6):821–825. https://doi.org/10.1016/j.nucmedbio.2012.02.004
16. Zhang Y, Stevenson GD, Barber C, Furenlid LR, Barrett HH, Woolfenden JM, Zhao M, Liu Z (2013) Imaging of rat cerebral ischemia-reperfusion injury using(99m)Tc-labeled duramycin. Nucl Med Biol 40(1):80–88. https://doi.org/10.1016/j.nucmedbio.2012.09.004
17. Liu Z, Larsen BT, Lerman LO, Gray BD, Barber C, Hedayat AF, Zhao M, Furenlid LR, Pak KY, Woolfenden JM (2016) Detection of atherosclerotic plaques in ApoE-deficient mice using (99m)Tc-duramycin. Nucl Med Biol 43(8):496–505. https://doi.org/10.1016/j.nucmedbio.2016.05.007
18. Gletsu N, Doan TN, Cole J, Sutliff RL, Bernstein KE (2005) Angiotensin II-induced hypertension in mice caused an increase in insulin secretion. Vasc Pharmacol 42(3):83–92. https://doi.org/10.1016/j.vph.2005.01.006
19. Kumar D, Trent MB, Boor PJ (1998) Allylamine and beta-aminopropionitrile induced aortic medial necrosis: mechanisms of synergism. Toxicology 125(2–3):107–115. https://doi.org/10.1016/S0300-483X(97)00168-6
20. Behmoaras J, Slove S, Seve S, Vranckx R, Sommer P, Jacob MP (2008) Differential expression of lysyl oxidases LOXL1 and LOX during growth and aging suggests specific roles in elastin and collagen fiber remodeling in rat aorta. Rejuvenation Res 11(5):883–889. https://doi.org/10.1089/rej.2008.0760
21. Zhang SH, Reddick RL, Piedrahita JA, Maeda N (1992) Spontaneous hypercholesterolemia and arterial lesions in mice lacking apolipoprotein E. Science 258(5081):468–471. https://doi.org/10.1126/science.1411543
22. Ishibashi S, Goldstein JL, Brown MS, Herz J, Burns DK (1994) Massive xanthomatosis and atherosclerosis in cholesterol-fed low density lipoprotein receptor-negative mice. J Clin Investig 93(5):1885–1893. https://doi.org/10.1172/JCI117179
23. Anidjar S, Salzmann JL, Gentric D, Lagneau P, Camilleri JP, Michel JB (1990) Elastase-induced experimental aneurysms in rats. Circulation 82(3):973–981. https://doi.org/10.1161/01.CIR.82.3.973
24. Freestone T, Turner RJ, Higman DJ, Lever MJ, Powell JT (1997) Influence of hypercholesterolemia and adventitial inflammation on the development of aortic aneurysm in rabbits. Arterioscler Thromb Vasc Biol 17(1):10–17. https://doi.org/10.1161/01.ATV.17.1.10
25. Daugherty A, Manning MW, Cassis LA (2000) Angiotensin II promotes atherosclerotic lesions and aneurysms in apolipoprotein E-deficient mice. J Clin Investig 105(11):1605–1612. https://doi.org/10.1172/JCI7818
26. Zhao M (2011) Lantibiotics as probes for phosphatidylethanolamine. Amino Acids 41(5):1071–1079. https://doi.org/10.1007/s00726-009-0386-9
27. Johnson SE, Li Z, Liu Y, Moulder JE, Zhao M (2013) Whole-body imaging of high-dose ionizing irradiation-induced tissue injuries using 99mTc-duramycin. J Nucl Med 54(8):1397–1403. https://doi.org/10.2967/jnumed.112.112490
28. Yamanouchi D, Morgan S, Stair C, Seedial S, Lengfeld J, Kent KC, Liu B (2012) Accelerated aneurysmal dilation associated with apoptosis and inflammation in a newly developed calcium phosphate rodent abdominal aortic aneurysm model. J Vasc Surg 56(2):455–461. https://doi.org/10.1016/j.jvs.2012.01.038
29. Ailawadi G, Moehle CW, Pei H, Walton SP, Yang Z, Kron IL, Lau CL, Owens GK (2009) Smooth muscle phenotypic modulation is an early event in aortic aneurysms. J Thorac Cardiovasc Surg 138(6):1392–1399. https://doi.org/10.1016/j.jtcvs.2009.07.075
30. Kotze CW, Menezes LJ, Endozo R, Groves AM, Ell PJ, Yusuf SW (2009) Increased metabolic activity in abdominal aortic aneurysm detected by 18F-fluorodeoxyglucose (18F-FDG) positron emission tomography/computed tomography (PET/CT). Eur J Vasc Endovasc Surg 38(1):93–99. https://doi.org/10.1016/j.ejvs.2008.12.016
31. Truijers M, Kurvers HA, Bredie SJ, Oyen WJ, Blankensteijn JD (2008) In vivo imaging of abdominal aortic aneurysms: increased FDG uptake suggests inflammation in the aneurysm wall. J Endovasc Ther 15(4):462–467. https://doi.org/10.1583/08-2447.1
32. Sakalihasan N, Van Damme H, Gomez P, Rigo P, Lapiere CM, Nusgens B, Limet R (2002) Positron emission tomography (PET) evaluation of abdominal aortic aneurysm (AAA). Eur J

Vasc Endovasc Surg 23(5):431–436. https://doi.org/10.1053/ejvs.2002.1646
33. Turner GH, Olzinski AR, Bernard RE, Aravindhan K, Boyle RJ, Newman MJ, Gardner SD, Willette RN, Gough PJ, Jucker BM (2009) Assessment of macrophage infiltration in a murine model of abdominal aortic aneurysm. J Magn Reson Imaging 30(2):455–460. https://doi.org/10.1002/jmri.21843
34. Klink A, Heynens J, Herranz B, Lobatto ME, Arias T, Sanders HM, Strijkers GJ, Merkx M, Nicolay K, Fuster V, Tedgui A, Mallat Z, Mulder WJ, Fayad ZA (2011) In vivo characterization of a new abdominal aortic aneurysm mouse model with conventional and molecular magnetic resonance imaging. J Am Coll Cardiol 58(24):2522–2530. https://doi.org/10.1016/j.jacc.2011.09.017